Fabrication and Modeling of Piezoelectric RF MEMS Resonators

Andrew Potter
Department of Physics and Division Engineering – Brown University
Advisor: Gianluca Piazza, PhD

Abstract

Resonators serve as essential components in radio-frequency (RF) electronics, forming the backbone of filters and tuned amplifiers. However, traditional solid state or mechanic implementations of resonators and filters tend to be bulky and power hungry, limiting the versatility of communications, guidance, and avionics systems. Micro-electro-mechanical systems (MEMS) are promising replacements for traditional RF circuit components. In particular Piazza, et al. has demonstrated high performance RF MEMS resonators utilizing thin film structures of piezoelectric aluminum-nitride (AlN) [2]. These AlN films have been previously patterned using chemical wet-etching techniques, whose isotropic nature results in mask undercutting and sidewall sloping. This paper demonstrates that inductively coupled plasma (ICP) etching results in a cleaner, straighter etch profile. Furthermore, the effects of sloped sidewalls are investigated through finite element simulations for ordinary and high-mode resonator structures. It is shown that sidewall sloping degrades resonator efficiency and performance.

Table of Contents

1. Introduction

1.1 – Piezoelectric RF MEMS Resonators

1.1.1 – Overview

Modern radio-frequency (RF) communications applications increasingly demand flexibility, low power consumption, and noise immunity. The Defense Advanced Research Projects Agency (DARPA) has recently shown interest in developing systems capable of hopping among multiple transmission and reception frequency bands. However, traditional RF circuit components tend to be bulky and power hungry limiting the durability, portability, and performance of RF devices. In particular, these limitations render a traditional implementation of a frequency agile system unfeasible. Because they offer superior performance, require less space, and are easier to integrate with silicon technology, micro-electro-mechanical systems (MEMS) devices have shown significant promise as replacements for traditional solid state and mechanical components in RF applications [1].

Resonators, which respond only to a narrow range of frequencies, provide the frequency selectivity necessary for any tuned circuit, and form the backbone of filters and tuned amplifiers. Figure 1.1 below shows the response of a typical piezoelectric resonator:
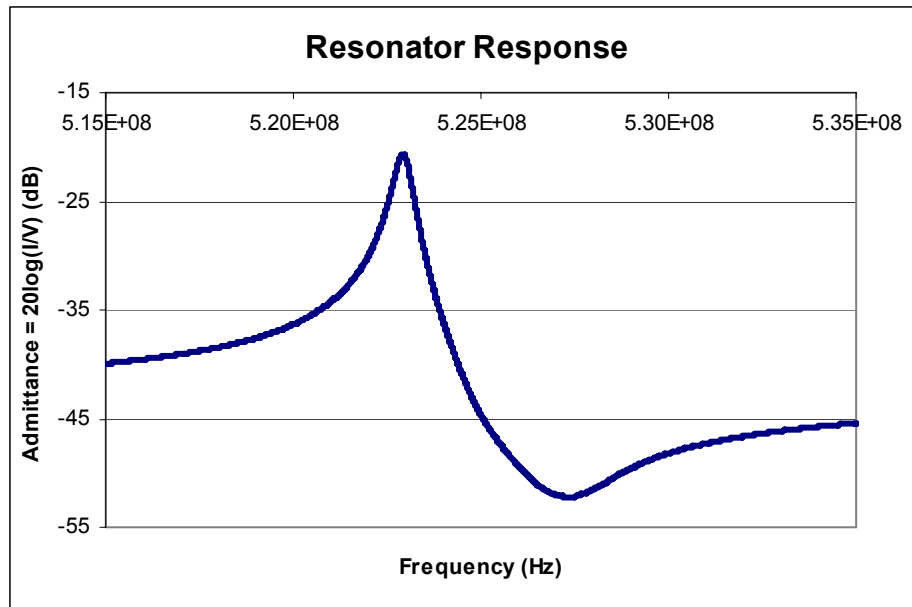

Figure 1.1 – Admittance plot of a typical resonator

where admittance (Y) is given by the logarithmic ratio of the output current and the applied voltage amplitudes:

$$Y = 20\log_{10}\left(\frac{I}{V}\right) \qquad (1)$$

The response is characterized by a resonance peak (at frequency f_1) followed by an anti-resonance peak (at frequency f_2) and the following two figures of merit: 1) the quality (Q) factor:

$$Q = \frac{f_{3dB2} - f_{3dB1}}{f_1} \approx \frac{Oscillation\_Energy}{Energy\_Dissipated} \qquad (2)$$

(where f_{3dB1} and f_{3dB2} refer to the cut-off frequencies on either side of the resonance peak), which characterizes the sharpness of the resonance peak, and 2) the k_t^2 value:

$$k_t^2 = \frac{\pi^2}{4}\left(\frac{f_2 - f_1}{f_2}\right) \qquad (3)$$

which measures the ratio of the mechanical response energy to the electrical input energy.

Several MEMS resonators based on a variety of actuation mechanisms, such as electro-static [5,6,7] forces or electro-thermal coupling [8], have been fabricated and tested. These devices have shown reasonable performance and quality (Q) factors (a measure of energy dissipation or, equivalently, sharpness in frequency response) in the range of 100-300 [1]; however, there remains room for improvement. Recent work by Piazza et Al has demonstrated high Q-factor (1500-2000), tunable MEMS resonators and oscillators utilizing piezoelectric aluminum nitride (AlN) [2,3,4]. In these devices, electrical signals couple with mechanical vibration modes of free-standing AlN structures through the piezoelectric effect. The geometry of such structures largely determines their resonance frequency; however, the resonator response can also be tuned by applying an external bias.

1.1.2 Fundamental Mode Devices

A simple one-bar resonator consists of a 2 μm thick bar of piezoelectric AlN sandwiched between two 200 nm thick platinum electrodes. The device is free-standing, suspended over a pit, and is tied to the wafer by thin anchors. During operation, an RF signal is applied to one of the electrodes. The piezoelectric layer then couples this electrical signal into a mechanical vibration, and subsequently back into an electrical signal at the other electrode. The mechanical structure has a natural fundamental resonance frequency determined by its geometry and will pass through signals near this resonance while suppressing others. Figure 1.2 below shows a cutaway view diagram of a 1-bar resonator structure. Similarly, figure 1.3 below shows a top-view scanning electron microscope (SEM) micrograph of this structure. Finally, table 1.1 below outlines the fabrication process for such a device [13].
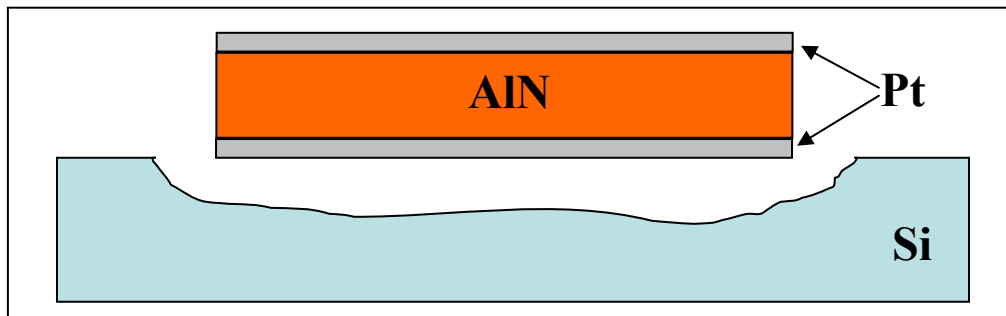

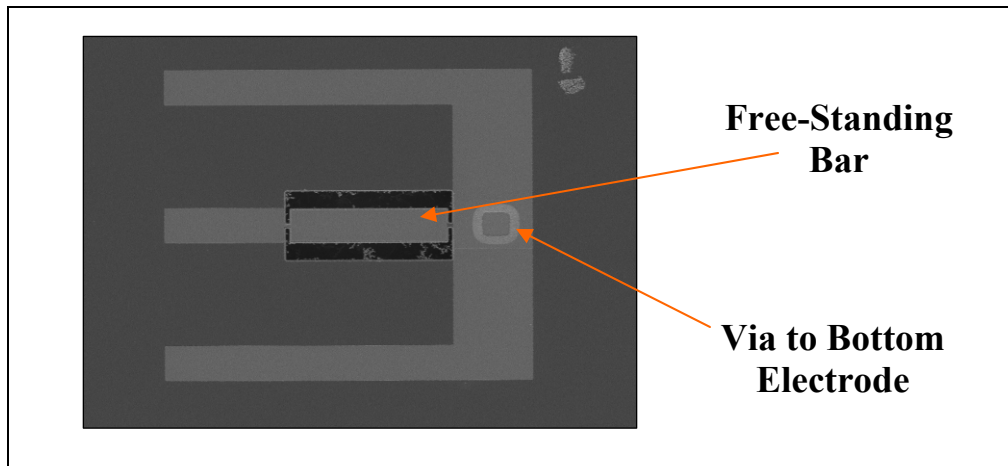Figure 1.2 – Cutaway view diagram of a bar resonator,

Figure 1.3 – Top-view SEM micrograph of a single bar resonator

	Description	Method/Comments
1	Bottom Electrode Deposition	Deposition: Plasma Enhanced Chemical Vapor Deposition (PECVD), 200nm
2	Bottom Electrode Patterning	Mask: Photoresist
3	AlN Deposition	Sputtered (Done at University of California-Berkeley), 2um film
4	Top Electrode Deposition/Patterning	Same as Bottom Electrode
5	Silicon Oxide	Sputtered or LPCVD, ~500-750nm (Serves as Masking Layer for AlN)
6	Patterning of Oxide Layer	Mask: Photoresist Etchant: CF_4 Plasma
7	Patterning of AlN Layer	Mask: Oxide Layer Etchant: BCl3, Cl_2, Ar Plasma
8	Device Release	Silicon underneath structure is etched away with CF_4 plasma, leaving the device free to vibrate

Table 1.1 – Fabrication Steps

1.1.3 Multi-fingered Devices

Higher frequency resonators can be achieved by exciting a suspended structure's higher order vibrational modes. Figure 1.4 below shows a side-view cutaway of a higher order device. The aluminum nitride bar is divided into multiple (in this case, 5) strips called fingers. The signal is applied to each, alternating polarity on each finger thus forcing a node between each finger and exciting a higher order mode.
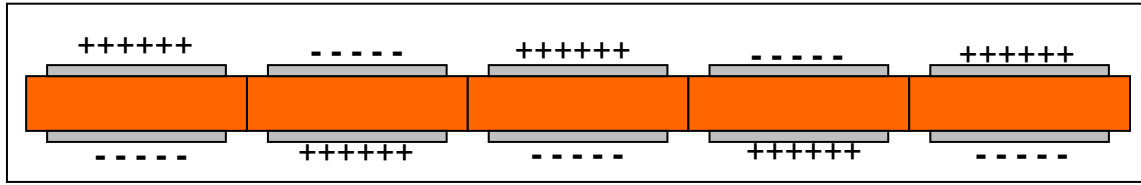
Figure 1.4 – Cutaway view of a 5-Fingered resonator structure, the pluses and minuses indicate the polarity of the signal applied to a particular finger. By choosing opposite polarities for adjacent fingers, a higher order mode of vibration is excited.
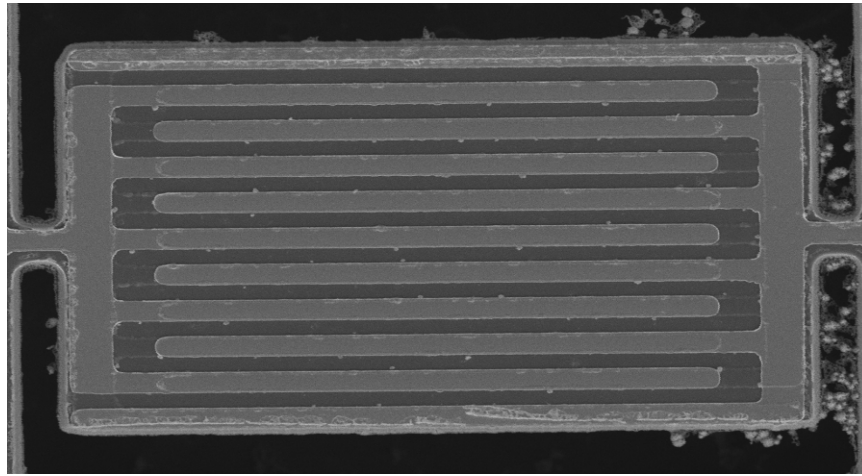

Figure 1.5 – SEM Micrograph of a multi-fingered device, black is the Si substrate, light gray is the platinum electrodes, dark grey is the AlN layer

Figure 1.5 above shows an SEM micrograph of a multi-fingered device. Two sets of alternate Pt strips interlace across the top to divide the structure into fingers. The bottom electrodes are patterned in the mirror image of the top electrodes, thereby achieving alternating polarities.

1.2 – ICP Etching

During the fabrication of piezoelectric RF MEMS switches and resonators, an AlN layer must be patterned into an appropriate geometry. However, photo-resistive polymers, typically used for such patterning, are susceptible to the chlorine-based etchants used to pattern AlN. As a result, a layer of sputtered silicon dioxide (SpOx) serves as a mask for the AlN layer. This oxide layer is in turn patterned using traditional photolithography (see table 1.1 above).

Chemical etching techniques typically have very good selectivity (i.e. they etch the exposed layer more quickly than they do the masking layer). However, these etches tend to be isotropic (etching outwards as well as down). As a result, the edges of the AlN structure have a non-vertical slope. Preliminary finite element analysis (FEM) simulations have indicated that such angled edges alter the vibrational modes of the

structure, coupling longitudinal oscillations with flexural oscillations. The excitation of these spurious modes induces energy dissipation through mechanisms such as thermo-elastic coupling [10], and hence decreases the device Q-factor. Furthermore, by coupling the electrical signal to flexural modes, the efficiency of the device is expected to decrease. Additionally, the thick material layers require relatively long etching times, which results in significant mask undercutting in isotropic chemical etches, and consequently reduces feature definition and edge sharpness. In order to address these issues, we are exploring inductively coupled plasma (ICP) reactive ion etching (RIE).

The term *plasma etching* encompasses a variety of techniques, each of which generally functions as follows: a chemically inert gas of neutral molecules (e.g. CF_4 or BCl_3) is split into more volatile ionic constituents which then bombard the substrate [11]. In ICP etching, an RF current signal is coupled to the gas chamber by a large inductive coil. This RF creates a transverse electrical field in the plasma chamber, which maintains the plasma and provides additional power [12]. The resultant process combines ballistic milling effects with chemical processing and generally achieves steeper side walls, and sharper feature definitions.

1.3 Project Goals

My initial goals for the project were as follows: 1) characterize the ICP etching process 2) model the effect of sidewall sloping on resonator performance, and 3) optimize the ICP process to improve the etching profiles. I initially hypothesized that sidewall sloping would reduce the efficiency and quality factor of the devices by inducing spurious flexural modes of vibration. Furthermore, I expected this effect to be more pronounced in devices with one or few fingers since the outer edges are more isolated from the bulk in a multi-fingered device and should therefore play less of a role in determining the mode-shape. Finally, I posit that decreasing the process pressure for ICP etching of AlN should decrease the amount of side-sloping, reasoning that at a lower pressure the etching ions suffer fewer collisions and therefore achieve higher speeds. I expected this to result in a more ballistic (and hence more vertical/anisotropic) etching process.

2. Simulations

2.1 – Setup and Methods

Finite Element Method (FEM) simulations were performed using the Piezo-solid module of COMSOL Multi-Physics Version 3.2. In each case, the software's direct parametric linear, frequency response solver was used.

Each of the simulated devices was 200um long, 50um wide, and 2um thick. Platinum layers were each 200nm thick. In order to reduce the computational complexity of the system, most of the simulations were two-dimensional, suppressing the longitudinal dimension. Approximating these structures as two-dimensional ignores the effects of the thin strips which anchor the resonator to the substrate. Furthermore, the

details of the interleaving platinum fingers in multi-fingered devices (see figure 1.5) are lost. However, despite these caveats, the resonators possess a large degree of longitudinal symmetry, and the two-dimensional simulation is expected to yield the qualitative effects of sidewall sloping.

In initial simulations, the platinum layer was omitted in order to reduce the number of degrees of freedom in the model system. However, omitting the platinum led to the generation of additional resonances in systems with sloped sidewalls (see figure 2.1 below). This secondary resonance peak split and separated from the primary resonance as the sidewall sloping increased. Inclusion of the metal layers in the model suppressed the spurious secondary normal mode corresponding to the second resonance.
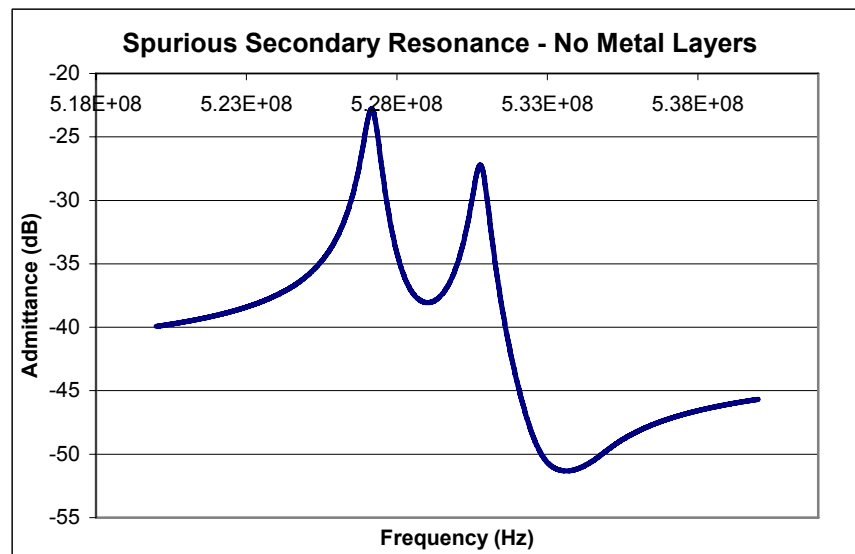

Figure 2.1 – Simulated Admittance Plot for a 5-Fingered Resonator with 76˚ sidewall slope – Notice the second resonance slightly displaced from the primary resonance.

In each simulation, a one-volt amplitude, time-harmonic voltage was applied to the top surface of the platinum layers. The material layers were artificially damped with a loss factor coefficient of 1/1000. The remaining surfaces were mechanically and electrically unconstrained. To extract admittance plots, the frequency response was simulated across a range of frequencies in 10 kHz increments, and for each frequency sample, the current density outflow was numerically integrated across the grounded surfaces.

2.2 – Results

Figure 2.2 below shows the effect of sidewall sloping on the resonance and anti-resonance frequency of a device. In the graphs above and for all that follow, sidewall angle refers to the angle between the sidewall and the bottom of the device, so that 90 degrees corresponds to flat sidewalls.
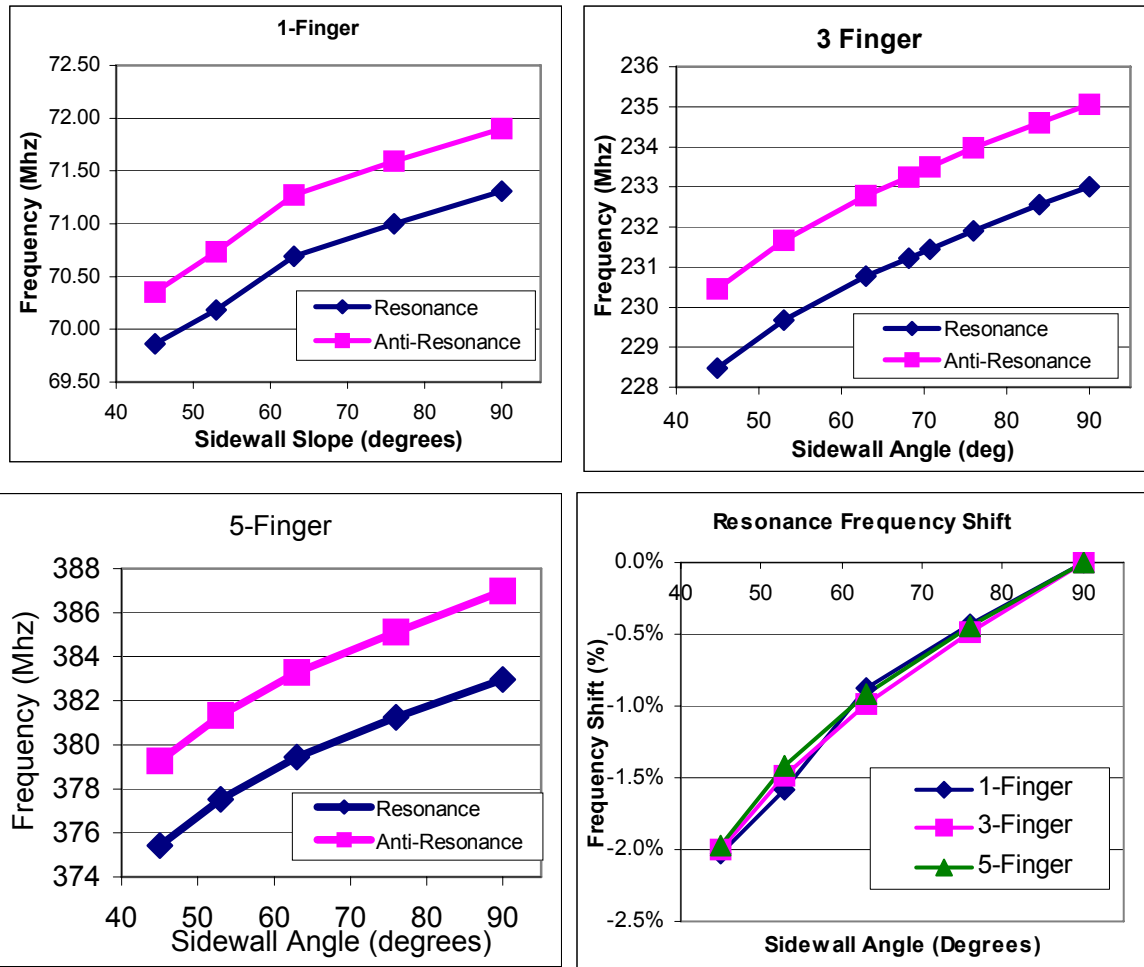
Figure 2.2 – Resonance Frequency Shift vs Sidewall Sloping for 1 (top-left), 3 (top-right), and 5 (bottom-left) fingers. (Bottom-Right) – Resonance frequency shift as a percentage of the flat sidewall resonance frequency.

In each case the resonance and anti-resonance frequencies decrease roughly linearly with decreasing sidewall angle (i.e. with more slope). To first order, this effect is accounted for by the additional mass in the sloped sidewalls (since a larger structure will tend to resonate at a lower frequency).

Figure 2.3 below shows the effect of sidewall angle on the k_t^2 values of one, three, and five fingered resonators. In each case sidewall sloping degrades the device electro-mechanical coupling efficiency, although the effect is far more pronounced in the single finger structures than in the multi-fingered devices.
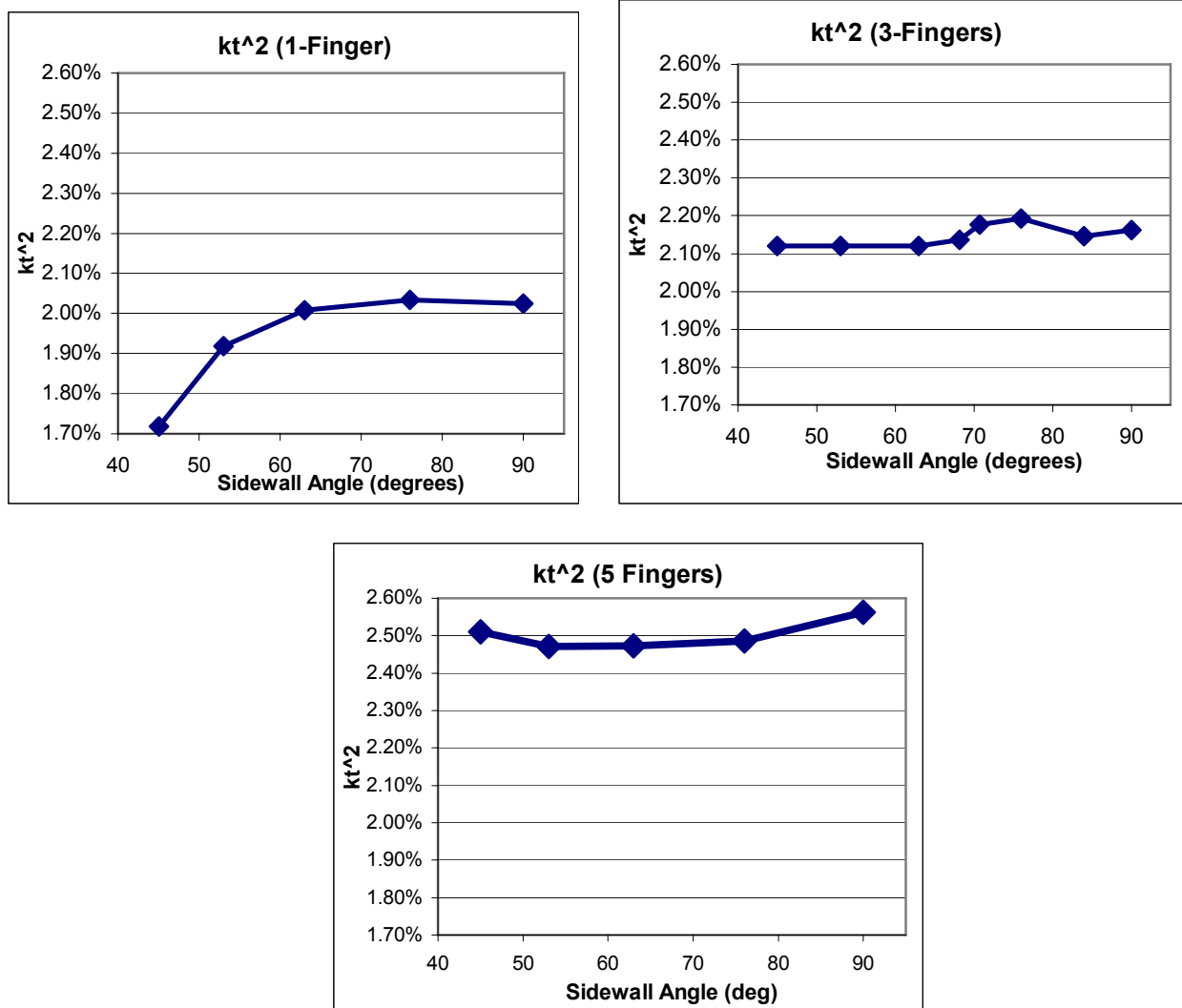
Figure 2.3 – k_t^2 vs. Sidewall Angle for 1 (top-left), 3 (top-right), and 5 (bottom-left) fingers (See equation (3) and the preceding discussion above)

3. Plasma Etching

3.1 – Materials and Methods

Characterization of an etching process consists of determining the effect of process parameters on the following two quantities: 1) etch rate – the rate at which the target material is consumed and 2) selectivity – the ratio of the etch rate of the target material to the masking layer.

To characterize the oxide etching process, two types of samples were prepared: 1) samples with a layer of sputtered oxide (SpOx) on top of a Si substrate (prepared at the University of Pennsylvania) and 2) samples with a layer of Low Pressure Chemical

Vapor Deposition (LPCVD) on top of a Si substrate (prepared at the University of California Berkeley). A 3.5um thick masking layer of photo-resist (Shipley 1827) was deposited on top of the oxide, was patterned, and developed. The thickness of the photo-resist layer was measured using a Tencor Instruments Alpha-step 200 profilemeter. The samples were then etched in a Trion Technology Phantom III ICP etcher using a CF_4 plasma, and the step height was measured again. During etching the chuck on which the samples were mounted was maintained at 12.4°C. Finally the remaining photo-resist was stripped off in an 85°C bath of PG Remover, and the resulting step height was measured. This final step height gives the amount of oxide etched during the ICP run. Similarly, the difference of the step height before and after ICP etching added to the final step height after photo-resist removal gives the amount of photo-resist consumed.   From these quantities the etch rate and selectivity are easily calculated. To reduce errors from process non-uniformities, care was taken to measure the same device for each of the above steps; 4-6 devices were tested for each sample, and the results presented below represent the averages across these devices.

To characterize the AlN etching rate, samples with patterned photo-resist on top of a stack of materials formed by sputtered oxide, AlN and the Si substrate were prepared. The oxide layer was patterned in buffered HF solution using the photo-resist as a mask. The photo-resist was then stripped in an 85° bath of PG Remover. The step height of the features was measured before and after ICP etching in a mixture of BCl_3, Cl_2, and Ar, and again after removing the remaining oxide with HF.   During etching the chuck on which the samples were mounted was maintained at 70°C. The first step height gives the thickness of the masking oxide layer, and the final gives the amount of AlN etched. Finally, using the same procedure described above for the oxide etch, the etch rate and selectivity were calculated.

3.2 – Silicon Oxide Results

Table 3.1 below contains the etch characterization results for sputtered oxide, and Table 3.2 contains the results for LPCVD oxide. Each of these results represents the average over multiple samples. The selectivity of sputtered oxide to photo-resist was ~1:3. As shown in the tables below, the etch rate and selectivity for sputtered oxide was most strongly affected by the Reactive Ion Etching (RIE) power used, with better selectivity achieved at lower power.

ICP [W]	RIE [W]	CF4 [sccm]	P [mT]	SiO2 Rate [nm/min]	PR Rate [nm/min]	1/Selectivity (PR:SiO2)	Comments
500	200	50	100	151	548	3.64	
500	100	50	100	101	315	3.13	
500	**50**	**50**	**100**	**52**	**154**	**3.00**	**Best Selectivity**
500	200	25	100	165	620	3.76	
500	25	45	100	53	163	3.10	5 sccm O2
500	25	45	150	23	73	3.65	5sccm O2

Table 3.1 – Sputtered Oxide Etching Rates (Bold Row represents best selectivity)

ICP [W]	RIE [W]	CF4 [sccm]	P [mT]	SiO2 Rate [nm/min]	PR Rate [nm/min]	1/Selectivity (PR:SiO2)	Comments
500	50	50	100	35	148	4.23	
500	100	50	75	103	420	4.08	Redeposition Film
500	100	50	100	78	301	3.88	
500	100	50	125	68	278	4.14	

Table 3.2 – LPCVD Oxide Etching Rates

The LPCVD oxide was more resilient to etching, and exhibited significantly reduced etch rates, and worse selectivity (~1:4). The best etching recipe for sputtered oxide resulted in inconveniently slow etching (<35nm/min) on the LPCVD samples. Increasing the RIE power gave more reasonable etch rates without sacrificing selectivity. Pressures below 75mT were also explored, however reducing the pressure below 100mT resulted in re-deposition of a chalky white film which rendered the samples unusable.

The best recipe overall in both cases was: 500W ICP, 50W RIE, 100mT Pressure, and 50sccm of CF_4. While lower power recipes resulted in better selectivity in some cases, the increased etch rates at 100W RIE power are more convenient and have similar selectivity.

3.3 – AlN Results

AlN Etching Conditions	
ICP (W)	500
RIE (W)	250
Cl2 (sccm)	25
BCl3 (sccm)	25
Ion Gauge (Torr)	5.0×10^{-5}
Pressure (mTorr)	75
Chuck Temp (C)	70
Ar (sccm)	10

Table 3.3 – Etching Recipe for AlN

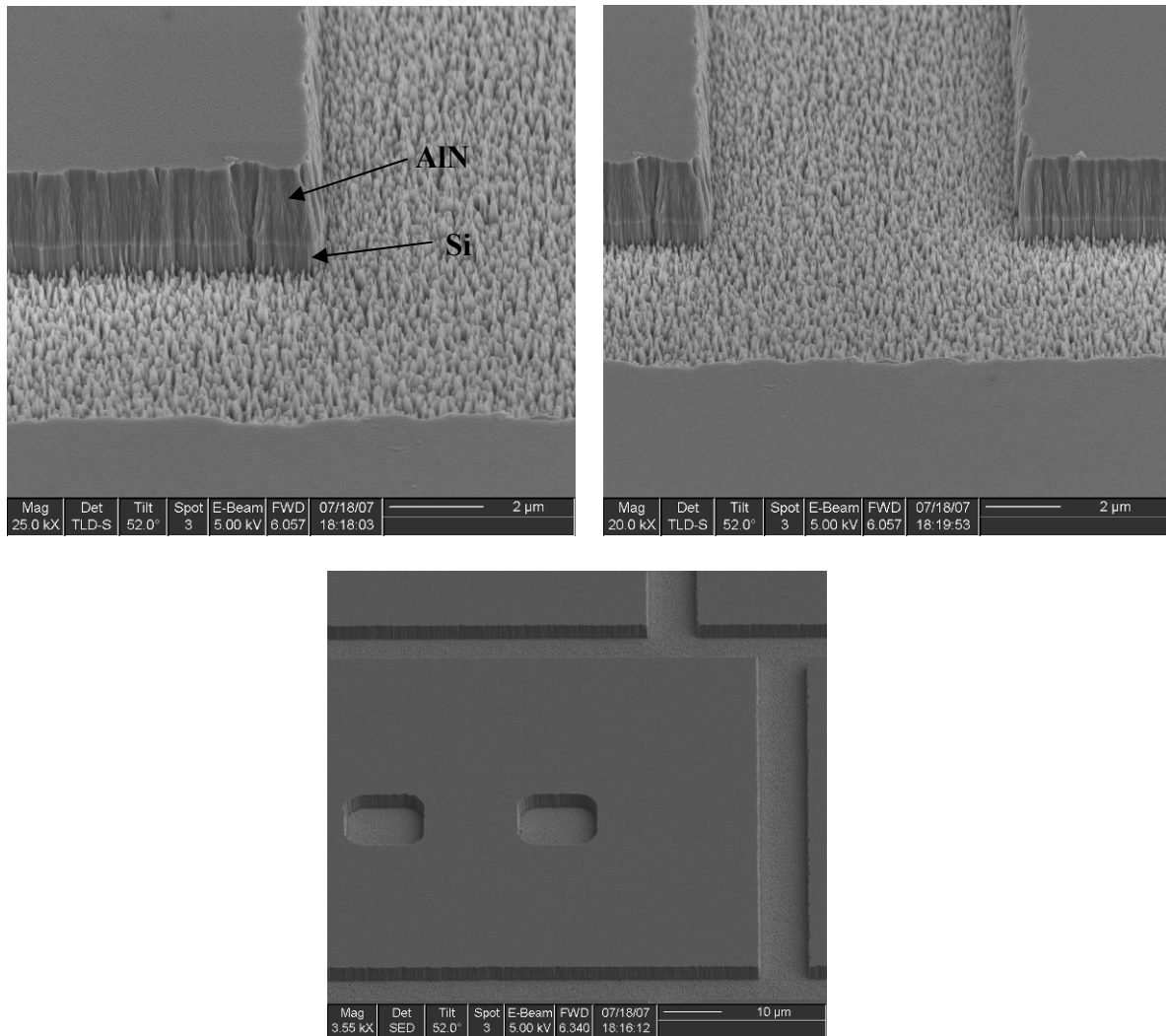| AlN Etching Results			
AlN Rate (nm/min)	223	**SpOx Selectivity**	4.23
SpOx Rate (nm/min)	53	**LPCVD Oxide Selectivity**	
LPCVD Oxide Rate (nm/min)	35		6.30

Table 3.4 – Etching Results for AlN

Figure 3.1 – SEM Micrographs of the ICP AlN etch profile. Close-up of sidewalls (Top right and left), Whole Device (Bottom); This sample was patterned using sputtered oxide as a masking layer.
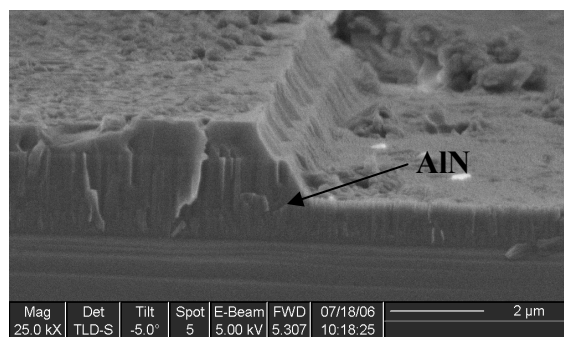

Figure 3.2 – SEM Micrograph of chemically etched AlN Profile

Tables 3.3 and 3.4 above list respectively the ICP conditions and the resulting average etch rates and selectivity of the process. The oxide layer serves as an effective mask and etches much less rapidly than the AlN. Selectivities for the sputtered oxide and the LPCVD oxide were 1:4 and 1:6 respectively. Again, the LPCVD oxide is much stronger than the sputtered oxide, and is more resilient to etching.

Figure 3.1 above shows three SEM micrographs of the AlN etching profile. The sample shown in these pictures has only patterned AlN on top of a Silicon substrate. Additionally, on this sample, a ten percent over etch was performed in order to ensure that the AlN was completely removed in the desired areas (see figure 3.1 top left). The sidewall profiles are quite straight, with only a small inclination. The scalloping, which is apparent on the sidewalls in the closeup shots is due to the buffered HF solution used to pattern the masking oxide.

As a contrast, figure 3.2 shows the AlN etch profile for chemical wet etching using KOH solution. The sidewall sloping for the wet-etch profile is much more pronounced than the corresponding dry-etch profile.

4. Discussion and Conclusion

Finite element simulations demonstrate that, as expected, sidewall sloping degrades resonator performance by shifting the resonance frequency and decreasing the coupling efficiency. However, single finger devices are much more strongly affected by sidewall sloping than multi-fingered devices (an intuitively appealing result, since only the outermost fingers are affected by sidewall sloping, whereas the inner fingers are somewhat mechanically insulated from the outer edges).

Furthermore, the etching characterization studies have proven that ICP etching of AlN with a masking layer of oxide is feasible. In order to pattern a 2 μm layer of AlN, the selectivities shown above require a minimum of 500 nm/340 nm of oxide and 1.5um/1.4um of photoresist when using sputtered/LPCVD oxide respectively. Finally, the etch profile of the plasma etched AlN samples is cleaner and has smaller sidewall sloping than the wet-etched samples.

Unfortunately, mechanical failures in the Trion ICP etcher rendered the machine unusable for four weeks of the summer. As a result of this inactivity, and of having to repeat all of the initial experiments to ensure that the etcher was properly functioning after its repairs, I did not have the chance to optimize the AlN etching process, explore the effect of various process parameters on the sidewall sloping, or experimentally verify the above simulations on physical devices. However, the ICP processes are now characterized well enough to use in the fabrication of future devices.

5. Acknowledgements

References

[1] Yao J J 2000 Topical review: RF MEMS from a device perspective *J. Micromech. Microeng.* **10** R9–R38

[2] G. Piazza, P.J. Stephanou, A.P. Pisano, "Single-Chip Multiple-Frequency AlN MEMS Filters Based on Contour-Mode Piezoelectric Resonators", *Journal of MicroElectroMechanical Systems,* vol. 16, no.2, pp. 319-328, April 2007.

[3] P. J. Stephanou , G. Piazza, C. D. White, M. B.J. Wijesundara, A. P. Pisano, "Piezoelectric aluminum nitride MEMS annular dual contour mode filter", *Sensors and Actuators A-Physical,* vol. A134, 2007.

[4] G. Piazza, P.J. Stephanou, A.P. Pisano, "Piezoelectric Aluminum Nitride Vibrating Contour-Mode MEMS Resonators", *Journal of MicroElectroMechanical Systems,* vol. 15, no.6, pp. 1406-1418, December 2006.

[5] Yao J J, Park S and DeNatale J 1998 High tuning-ratio MEMS-based tunable capacitors for RF communications applications *Tech. Digest, Solid State Sensor and Actuator Workshop* pp 124–7

[6] Young D J and Boser B E 1996 A micromachined variable capacitor for monolithic low-noise VCOs *Tech. Digest, Solid State Sensor and Actuator Workshop* pp 86–9

[7] Goldsmith C L, Malczewski A, Yao Z J, Chen S, Ehmke J and Hinzel D H 1999 RF MEMS variable capacitors for tunable filters Int. J. RF Microwave Comput.-Aided Eng. 9 362–74

[8] Feng Z, Zhang W, Su B, Harsh K F, Gupta K C, Bright V and Lee Y C 1999 Design and modeling of RF MEMS tunable capacitors using electro-thermal actuators Tech. Digest, 1999 IEEE MTT-S Int. Microwave Symp. pp 1507–10

[9] Zhang Q.Q., S.J. Gross, S. Tadigadapa, T.N. Jackson, F.T. Djuth and S. Trolier-McKinstry, *Sens. Actuators, A, Phys.* **105** (2003), p. 91.

[10] Lifshitz R. and M.L. Roukes, Thermoelastic damping in micro- and nanomechanical systems *Phys. Rev. B* **61**, 5600 -2000

[11] Coburn J. W., and H. F. Winters. Plasma Etching – A Discussion of Mechanisms. *Journal of Vacuum Science and Technology.* Vol. 16 Issue 2 (1979), 391-403.

[12] Hopwood J. Review of Inductively Coupled Plasma Etching. *Plasma Sources Science and Technology*. 1 (1992), 109-116.

[13] Piazza, G., P.J. Stephanou, and A.P. Pisano, Piezoelectric Aluminum Nitride Vibrating Contour-Mode MEMS Resonators. *Journal of Microelectromechanical Systems*. Vol. 15, No. 6 (2006), 1406-1417.